Spectroscopic measurements of electron density and temperature in polyacetal-capillary-discharge plasmas

C. A. Morgan* and H. R. Griem
Laboratory for Plasma Research, University of Maryland, College Park, Maryland 20742

R. C. Elton
Plasma Physics Division, Naval Research Laboratory, Washington D.C. 20375

(Received 4 June 1993)

Spectroscopic measurements were made of electron density and temperature histories in plasmas formed by 80-ns risetime, 6–16-kA peak current, pulsed discharges in 0.5- and 1-mm diameter, 1-cm-long polyacetal $(CH_2O)_n$ capillaries. Electron densities ($\lesssim 5\times10^{19}$ cm^{-3}) and temperatures ($\lesssim 50$ eV) in the capillary were inferred by fitting axial, spatially integrated, time-gated spectra taken of O VI $3p$-$4d$ and $3d$-$4f$ emission with theoretical Stark-broadened profiles that were corrected for optical-depth effects. Off-axis (at 45° to the capillary axis) time-gated spectra taken of C III $3p$-$3d$ and C IV $3s$-$3p$ emission from inside the hollow anode were used to infer the presence of a cooler ($T_e \lesssim 25$ eV), less dense ($N_e \lesssim 2\times10^{18}$ cm^{-3}) plasma just outside the capillary.

PACS number(s): 52.25.−b, 42.55.Vc, 52.70.Kz, 32.70.Jz

I. INTRODUCTION

Searching for gain at shorter wavelengths has always been an important aspect of laser research. Research and development of x-ray lasers has been motivated in part by the need for a greater understanding of the physics of the dense plasmas involved and in part by the promise of some direct applications [1–4]. These include x-ray microscopy and holography of biological samples, basic atomic physics, diagnostics of dense inertial confinement fusion (ICF) plasmas, and high-resolution photolithography. These and other potential applications of x-ray lasers are presented in greater detail in a recent monograph [1] which also serves as an important reference source and primer for the subject. Great progress has been made in the past decade [2,3,5] in achieving lasing action at short wavelengths, in bringing intensities up to saturation levels, and in conducting proof-of-principle experiments for certain applications. This success has been achieved using very large laser drivers as pump sources, and has generated renewed interest in the development of more compact, efficient and accessible ("tabletop") x-ray lasers. Several proposals for such a tabletop x-ray laser involve capillary discharges [6–9].

Capillary discharges were originally studied in fusion research [10–16] and as intense sources of continuum and line emission [17–23] for spectroscopy and soft-x-ray microscopy and lithography. Capillary plasmas are produced by electrical discharge through a small hole or slot in a solid insulator placed between two axial electrodes. The material in the plasma may come from ablation of the wall and electrodes, from a fill gas, or from an exploding wire [24,25] in the capillary. The values of the discharge conditions (e.g., current, charging voltage, discharge duration, and plasma electron density N_e and temperature T_e) have varied widely between experiments. These can range from currents of 10^{-6} A to 10^{-1} A in dc glow capillary discharges [26,27] (with $N_e \lesssim 10^9$ cm^{-3} and $T_e \leq 5$ eV) to currents and charging voltages of tens to hundreds of kA and kV, respectively, in transient (ns to μs time scale) capillary discharges. In the latter case N_e can be greater than 10^{22} cm^{-3} [24] and T_e can range from less than an eV [24] to greater than 200 eV [16].

One proposal [8] for a tabletop x-ray laser involves rapid cooling and three-body recombination [1,28] in a capillary-discharge plasma. A particular transition of interest in that regard is the C VI $H_\alpha(n=2-3)$ line at 18.2 nm from hydrogenic C^{5+} ions, for which recombination-pumped gain was reported in the 1980s from laser-produced plasmas [29–31]. There have been recent reports [32,33] of amplification on this line from a capillary-discharge experiment. The original experiment [32] involved discharges in polyacetal capillaries of between 0.5 and 1 mm diameter and 1 to 3 cm in length, and reported gains of 1.2 to 2.7 cm^{-1} in the form of intense $\lesssim$1-ns spikes of emission at 18.2 nm. The spikes were seen near the peak of the second half cycle of the low-inductance ($\sim$15 nH), low-voltage ($\sim$9 kV), 240-ns-period discharge. They were observed using a 1-m grazing-incidence, extreme-ultraviolet monochromator equipped with a scintillator and photomultiplier. The conclusion of gain was based on (a) observations of increases in amplitude with capillary length, and (b) a narrower solid angle of emission than that of a nearby O VI line at 18.4 nm. Improvements were made to the original experiment [33] and spikes at 18.2 nm were again observed. Support for the gain interpretation was also provided [33] by the observation of a significant enhancement of the 18.2-nm spike amplitude with the addition of a 12% reflectivity multilayer plane mirror at the end opposite to that of observation. A variety of other work in

*Present address: Bldg. 221, National Institute of Standards and Technology, Gaithersburg, Maryland 20899.

progress worldwide involving capillary plasmas related to x-ray-laser research is discussed in Ref. [34]. A study of the temporal evolution of electron density in 110-ns full width at half maximum (FWHM) discharges at higher voltages in 1-cm-long, 0.5- to 1.5-mm-diameter, polyacetal capillaries has recently been presented [35]. Diagnostic measurements of open-geometry capillary plasmas have also been presented recently [36,37].

Recombination-pumped gain on the H_α line of C VI depends strongly on the conditions of both electron density and temperature [1,38,39]. An electron temperature of $T_e \gtrsim 160$ eV is necessary to fully ionize carbon to C^{6+}. The C^{6+} ions must then experience a rapid drop in electron temperature to $T_e \lesssim 40$ eV on a time scale shorter than or on the order of that needed to populate the upper laser level by recombination and cascade. Electron-collisional mixing of the upper and lower levels defines an upper limit on electron density beyond which population inversion and gain are quenched. In practice, the electron density should be somewhat below this limit, which, in this case leads to a requirement that $N_e \lesssim 10^{19}$ cm^{-3}. A lower limit is set by the fact that gain falls off strongly with decreasing N_e in the region where collisional mixing is negligible. The presence or absence of absorption in the plasma in the hollow anode region beyond the capillary could determine whether amplification on the H_α line of C^{5+} in the capillary plasma would be observable. In these contexts, diagnostic analysis of both of these plasmas is important.

We report here on spectroscopic observations made of polyacetal-$(CH_2O)_n$-capillary discharges with parameters similar to those for which the amplified bursts of emission were originally reported [32]. Separate spatially integrated, time-resolved electron density and temperature measurements were made of the plasmas in the capillary (using O VI $3p$-$4d$ and $3d$-$4f$ line emission) and in the hollow graphite anode (using C III $3p$-$3d$ and C IV $3s$-$3p$ line emission). The results of these measurements ($N_e \lesssim 5\times10^{19}$ cm^{-3}, $T_e \lesssim 50$ eV for the capillary plasma and $N_e \lesssim 2\times10^{18}$ cm^{-3}, $T_e \lesssim 25$ eV for the anode plasma) did not conform to the pattern necessary for recombination-pumped gain on the H_α line of C^{5+}. In particular, no evidence was seen for the $\gtrsim 160$-eV electron temperature necessary to fully ionize the carbon to C^{6+}. Nevertheless, because our measurements were spatially integrated, we cannot exclude the possibility that the necessary pattern of conditions was fulfilled in some small portion of the plasma.

II. EXPERIMENT

A. Discharge circuit and parameters

The capillary-discharge circuit [Fig. 1(a)] consisted of a pair of 0.05-μF, 20-nH, 50-kV-rated, plastic-package capacitors in parallel with a transmission line of much lower inductance. The transmission line leads to two coaxial cylindrical hollow (1 mm internal diameter, 6 mm external diameter, 5 mm long) graphite electrodes, on either side of, and coaxial with a 0.5- or 1-mm-diameter, 1-cm-long, polyacetal capillary. The total circuit capacitance (C) and inductance were ~ 0.1 μF and 27 nH, respectively. The discharge volume was pumped to a pressure of $\lesssim 10^{-5}$ Torr. The anode was grounded and the cathode was charged negatively. The applied potential was maintained across the insulating capillary until a trigger pulse produced a surface flashover which initiated the discharge. This trigger consisted of a -10 to -15 kV (with respect to the cathode) high-voltage pulse applied to a side-mounted, tungsten pin adjacent to the cathode. The range of charging voltage (V_C) used in this experiment was 3.5 to 16 kV, which corresponded to 0.6 to 11 J of stored energy ($E_C = \frac{1}{2}CV_C^2$) and 6 to 23 kA peak current in the circuit. The energy density in the capillaries ranged from 80 to 5000 J cm^{-3}, where energy density is defined as the ratio of E_C to capillary volume.

A Rogowski loop [34] was used to monitor the evolution of the discharge current. A time-averaged circuit resistance of $R \sim 0.27$ Ω was inferred from the damping of the current wave form. This is comparable to an estimate of $R_\perp \sim 0.7$ Ω obtained from an expression for the perpendicular resistivity [27] of the plasma:

$$R_\perp = \frac{4\eta_\perp l}{\pi D_{\rm cpl}^2}\ , \tag{1}$$

$$\eta_\perp = 1.03\times10^{-2} Z T_e^{-3/2} \ln\Lambda\ \Omega\,{\rm cm}\ , \tag{2}$$

where $\ln\Lambda$ is the Coulomb logarithm, $Z = 3$ is the average

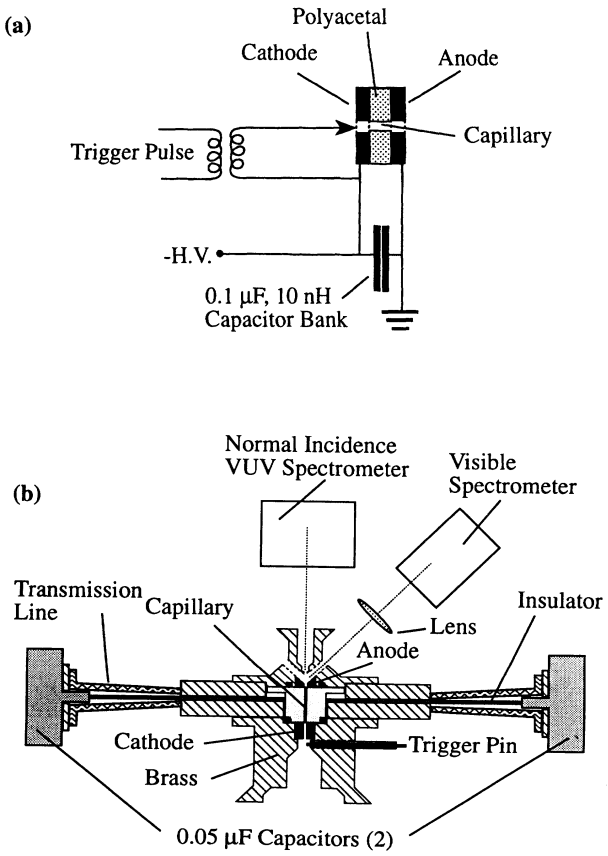

FIG. 1. Circuit (a) and experimental setup (b).

age ion perturber charge, $l=1$ cm is the length of the capillary, $D_{\rm cpl}=0.05$ cm is the capillary diameter, and where it is assumed that $N_e=2.5\times10^{19}$ and $T_e=20$ eV [34]. It should be noted that the small value for $\ln\Lambda$ $\rm cm^{-3}$ (≈4) implies that the above estimate of Spitzer resistivity was made for plasma conditions where it may no longer be very accurate.

The rate at which capillaries eroded (and their diameters increased) depended strongly on material, initial diameter, and applied voltage [34]. The energy required to ionize a homogeneous, $N_e=5\times10^{19}$ $\rm cm^{-3}$ plasma filling a 0.5-mm-diameter, 1-cm-long capillary to O^{5+}, C^{4+}, and H^+, in proportion to their presence in polyacetal, was estimated at ≈0.8 J. The energy needed to heat the ions and electrons to 30 eV was estimated at ≈0.5 J. Thus the energy needed to form the plasma (≈1.3 J) represented a minor fraction of the 6 J of energy stored in the circuit at $V_C=11$ kV. The bulk of the remaining stored energy was dissipated in the form of oxygen-ion radiation, coupled into heating the capillary and electrodes. By depriving the plasma of energy that would have otherwise gone into ionization and heating, this severe radiation loss served to significantly depress temperatures and ionization stages in the plasma. In heating of the capillary wall, the radiation loss also increased the influx of cooler material, further keeping temperatures and ionization stages lower.

Use of a capillary composed of polyethylene $(CH_2)_n$, which does not contain oxygen or other strong radiators, would tend to couple the available energy more effectively into heating and ionizing the plasma, leading to higher temperatures and ionization stages [40]. Results have been reported [41] for polyacetal versus polyethylene capillaries. Heating a lesser amount of material using capillaries with less ablative walls [22] or a fill gas [42], and faster [9] (~10 ns, before wall conduction of the discharge current becomes established), megavolt-level discharges, also lead to higher temperatures.

B. Setup for capillary plasma measurements

A 1-m normal-incidence, vacuum-ultraviolet spectrometer was placed end-on to the capillary at a distance of 0.53 m. The discharge was viewed through a 5-mm-long, 1-mm-diameter hole in the anode [Fig. 1(b)]. The spectrometer was equipped with a 2400-groove/mm osmium-coated spherical diffraction grating of ~1 m radius of curvature. A microchannel-plate–phosphor–fiber-optic bundle backed by a reticon linear diode array [43] was mounted in the plane of the Rowland circle. The spectrometer inverse dispersion and instrumental FWHM corresponded, on the reticon, to ~0.0108 nm/channel and ~6.5 channels, respectively. The microchannel plate was gated by a high voltage ~-660-V, 12-ns pulse atop a -500-V dc bias voltage, triggered by an attenuated Rogowski coil signal with variable delay with respect to the discharge. The error in gate timing was $\approx\pm2$ ns. Time-gated spectra near the O VI $3d$-$4f$ and $3p$-$4d$, 51.97- and 49.84-nm lines were taken at a variety of times with respect to the discharge, for $V_C=3.5$, 6.0, 8.5, and 11 kV and $D_{\rm cpl}=1$ and 0.5 mm. Fits described in detail below (Fig. 3) were then made to that portion of the spectrum (~49–53 nm).

This setup was modified, as follows, to permit time-resolved, spatially averaged measurements of integrated relative intensity in O VI $2s$-$2p$, O IV $2s^22p$-$2s2p^2$, and O III $2s^22p^2$-$2s2p^3$ lines. A P-terphenyl- (scintillator) coated quartz vacuum window and a Hamamatsu H3164 photomultiplier tube assembly were mounted on the spectrometer. The exit slit covered a ~0.22-nm wavelength interval. The data were obtained using the storage oscilloscope for the same range of discharge conditions as mentioned above. Traces were recorded for several shots, taken at roughly that wavelength interval, to scan over the lines of interest. The traces were numerically smoothed with a 20-ns integration time. A similarly smoothed background trace was subtracted; the resulting traces corresponding to a particular line were added to give the measurements of integrated relative intensity of the lines.

C. Setup for anode plasma measurements

The experimental setup for the off-axis observations of the plasma inside the anode is depicted in Fig. 1(b). This plasma, just outside the capillary, was viewed through a 1-mm-diameter hole drilled in the anode at 45 degrees to the axis. A quartz lens imaged that region, with 1:1 magnification, onto the entrance split of a 0.6-m visible spectrometer. An optical multichannel analyzer (OMA) detector was coupled to the image plane of the spectrometer. A 512×512 vidicon array constituted the OMA head. No spatial resolution was possible.

The spectrometer was equipped with a 1200-groove/mm diffraction grating, giving a spectral inverse dispersion of ~0.032 nm/channel. The instrumental FWHM was ~3.5 channels or 0.11 nm. The spectrometer was mounted on a platform, with micrometer adjustment perpendicular to the observation axis. With each capillary replacement several initial shots were taken at a low voltage (6 kV) for alignment purposes.

The intensifier of the OMA was gated with a negative ~1.25-kV, 60-ns pulse from a Krytron circuit [44]. The relative timing of the gate pulse and the discharge was independently adjustable. The Rogowski coil signal triggered the OMA detector controller to download the time-gated spectral data to an OMA console. From there the data were transferred to a computer. Data processing consisted of subtracting an OMA dark current spectrum, wavelength calibration, and fitting of the spectral line shapes to Voigt profiles.

III. RESULTS AND DISCUSSION

A. Capillary plasma

A series of axial, time-gated, spatially integrated vacuum-ultraviolet spectra of O VI $3p$-$4d$, 49.84-nm and $3d$-$4f$, 51.97-nm [45] emission were taken for each of several discharge conditions (8.5- and 11-kV discharges in 1.0-mm-diameter capillaries and 3.5-, 6.0-, 8.5, and 11-kV discharges in 0.5-mm-diameter capillaries). These spectra were used to infer time histories of electron density

[34] ($N_e \lesssim 5\times10^{19}$ cm^{-3}) and temperature [34] ($T_e \lesssim 50$ eV). These results involved the application of a more complicated interpretation of Stark-broadening theory [35] than that used for the C IV 3*s*-3*p* lines (Sec. III B 1). This theory predicts a series of Doppler-broadening Stark profiles of O VI 3*d*-4*f*, 3*p*-4*d* and their forbidden components in the wavelength range 48–54 nm, corresponding to a set of electron densities in the range of 1.0×10^{18}–6.0×10^{19} cm^{-3}. These profiles were used in fitting the experimental spectra.

1. N_e and T_0 measurements

The electron density values deduced were used in conjunction with a collisional radiative equilibrium code [34] to estimate the corresponding electron temperatures. The details of the fitting process were as follows: (1) A profile $L(\lambda)$, chosen from among those available in the series, was modified to take into account effects of optical depth and instrumental broadening. (2) The resulting profile was added to a straight line background. (3) A number of Lorentzian profiles, each centered at a different wavelength, were added so as to fit other lines (O III, C III, and other impurities) in the experimental spectrum. (4) The fit parameters involving N_e and optical depth were varied away from the "best fit" values to establish their range of probable error.

The fitting process was simplified by the fact that in most cases the other lines mentioned above made only a minor contribution to the experimental spectra. This permitted the parameters for N_e and optical depth to be determined independently from those of the other lines and the straight line background. Fitting was far more complicated for several spectra taken towards the beginning and end of O VI emission for each discharge condition, where the contributions of other nearby lines were comparable to or greater than those of O VI, and where some of the lines (in particular a C III 49.92-nm line) were blended with the O VI lines.

The modification of the original Doppler-broadened Stark profile $L(\lambda)$ for optical depth and instrumental broadening was performed as follows: An optical depth profile $T(\lambda)$ was calculated using

$$T(\lambda)=\frac{T_0 L(\lambda)}{P_L}\ , \tag{3}$$

where P_L is the value of $L(\lambda)$ at the peak of the O VI 3*d*-4*f* multiplet. T_0, the optical depth at the peak of the O VI 3*d*-4*f* multiplet, is the optical depth fit parameter. The profile modified for optical depth effects $L_T(\lambda)$ is given by the solution to the radiative transfer equation, assuming a homogeneous plasma [46]:

$$L_T(\lambda)=S\{1-\exp[-T(\lambda)]\}\ , \tag{4}$$

where the source function S is taken to be constant over this wavelength interval. This result (L_T) is then convolved with the instrumental Voigt profile $G(\lambda')$:

$$L_{TI}(\lambda)=\int_{-\infty}^{\infty} G(\lambda')L_T(\lambda-\lambda')d\lambda' \tag{5}$$

to give the fully modified profile $L_{TI}(\lambda)$. The effects of N_e and T_0 on the modified spectral profile $L_{TI}(\lambda)$ [and ultimately on the fitting profile $F(\lambda)$] were somewhat linked. Increasing N_e or T_0 had the same effect of increasing the widths of these features. Opposite effects were seen on the ratio R of peak intensities of the O VI 3*p*-4*d* and 3*d*-4*f* features, in that increasing N_e reduces R while increasing T_0 increases R. That dependence of the modified spectral profile on electron density and optical depth at the 3*d*-4*f* line center is illustrated in Fig. 2. The changes in the optically thin line shapes with increasing N_e in Figs. 2(a) and 2(b) are noted as follows: (1) Both features become broader, particularly the 3*p*-4*d* multiplet whose principal components are shifted in opposite directions as well as broadened, (2) the 3*d*-4*f* line shape becomes increasingly affected by the forbidden component appearing on the longer wavelength side of the line, and (3) the ratio of peak intensities R decreases appreciably, whereas the ratio of integrated intensities remains constant. This is consistent with the greater increase in broadening of the 3*p*-4*d* multiplet. With increasing optical depth the relevant changes in line shapes corresponding to $N_e=1.0\times10^{19}$ cm^{-3} [Figs. 2(c) and 2(d)] are (1) both 3*p*-4*d* and 3*d*-4*f* multiplets are increasingly broadened, (2) the 3*d*-4*f* line shape becomes increasingly affected by the 3*d*-4*d* forbidden component appearing on the longer wavelength side of the line, and (3) the ratio R increases significantly from ≈0.15 in the optically thin case, to greater than 0.6 for optical depth $T_0=6.0$. A sample "best fit" to an experimental spectrum, for $N_e\approx3.2\times10^{19}$ cm^{-3} and $T_0\approx3.4$, appears in Fig. 3. Figure 4 shows the results from the fitting process of N_e

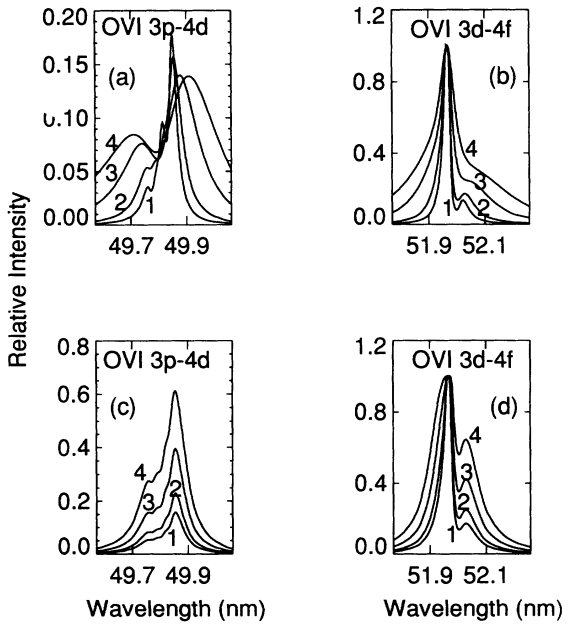

FIG. 2. Dependence of the O VI 3*p*-4*d* and 3*d*-4*f* theoretical line shapes on electron density N_e and optical depth T_0 at the O VI 3*d*-4*f* line center. The values of N_e represented by 1, 2, 3, and 4 on (a) and (b) were 0.5, 1.0, 3.0, and 6.0×10^{19} cm^{-3}, respectively. The values of T_0 similarly represented on (c) and (d) were 0.001, 1.0, 3.0, and 6.0.

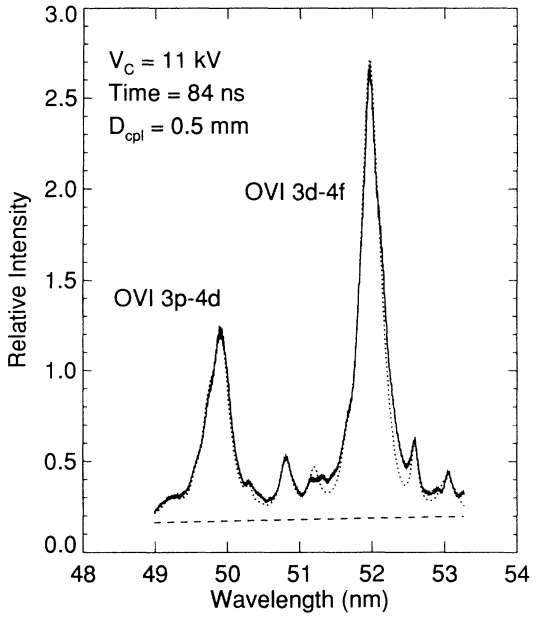

FIG. 3. Example of a fit (dotted line) to a time-gated, spatially integrated spectrum in the region of 49 to 53 nm.

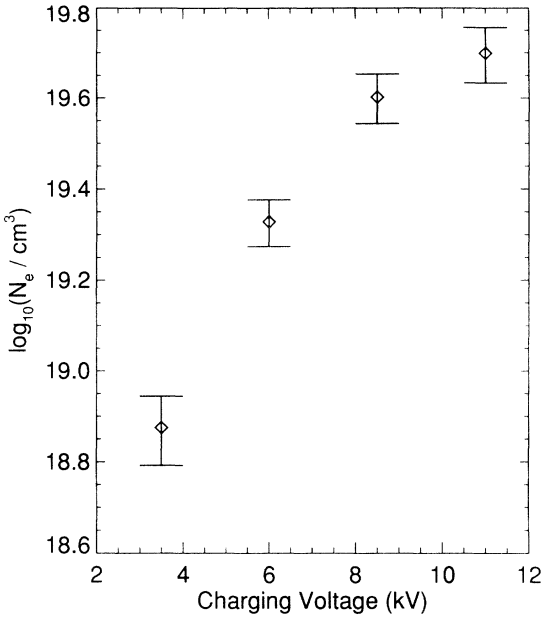

FIG. 5. Peak measured electron density plotted versus charging voltage in 0.5-mm capillaries.

and T_0 versus time, for 11-kV discharges in 0.5-mm capillaries. The N_e histories for all of the observed discharge conditions [34] were seen to possess the same general shape. That shape consisted of a rise to a peak value followed by a decrease within the first half cycle of the discharge. Peak N_e occurred 30–40 ns earlier in the case of discharges in 0.5-mm-diameter capillaries than for the 1-mm capillaries; it was a monotonic increasing function of charging voltage (Fig. 5) or stored energy. Features similar to these have been reported [35] from discharges in polyacetal of greater voltage and larger capillary diameter.

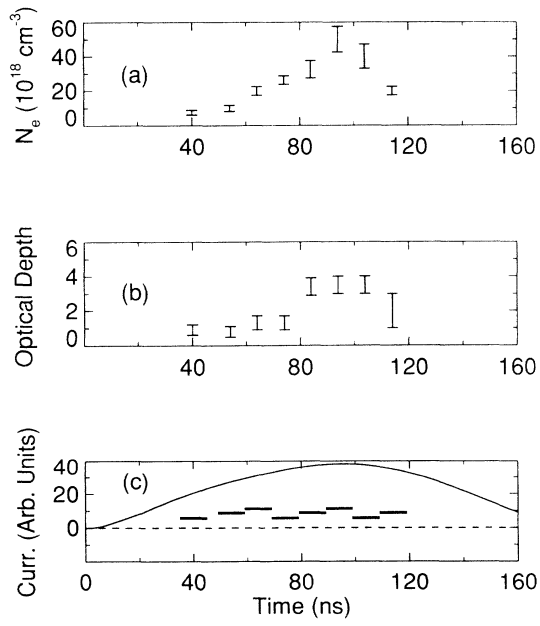

FIG. 4. Results for electron density (a) and optical depth (b) at O VI $3d$-$4f$ line center derived from fitting spatially integrated, time-gated vacuum-ultraviolet spectra in the spectral region of 49 to 53 nm, taken of 11-kV discharges in 0.5-mm capillaries. Current trace (c) with microchannel-plate gate windows (black bars).

2. T_e measurements

Ranges of T_e consistent with the values of N_e and T_0 presented above were estimated with the help of a steady-state, collisional radiative equilibrium code which was developed [34] to predict level populations (e.g., N_{2p}, N_{3d}, and N_{4f}) in O VI over a range of N_e and T_e (1.0×10^{18} to 6.0×10^{19} cm^{-3} and 10 to 50 eV, respectively) in plasmas derived from polyacetal. The predicted population density of the $3d$ level, $N_{3d}(N_e,T_e)$, was used to further predict the optical depth at the O VI $3d$-$4f$ line center, $T_0(N_e,T_e)$. Ranges of T_e consistent with each set of measured values for N_e and T_0 were read from a contour plot (Fig. 6) of the code prediction for $T_0(N_e,T_e)$.

Values of collisional excitation and deexcitation rate coefficients used in the code were scaled from measurements [47,48] and calculations [49] of other lithiumlike ions. The effects of uncertainty in the radiative and collisional rate coefficients are not expected to be large, because for the above range of N_e and T_e, the level populations in O VI do not depart radically from local thermodynamic equilibrium values, given that the collision limit quantum number n' [1,46] is between 3 and 4.

The results for T_e in 8.5- and 11-kV discharges with 0.5-mm-diameter capillaries are shown in Fig. 7. The possible value of T_e at any given time generally [34] fell within two intervals, a narrow one in the region of 11 to 15 eV and a much wider one in the region of 20 to 40 eV. These intervals represent the range of T_e on the contour

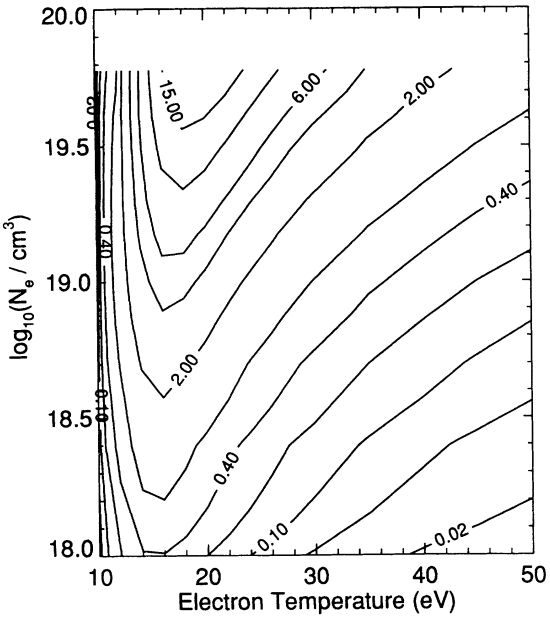

FIG. 6. Contours of the collisional radiative equilibrium code predictions of optical depth at O VI $3d$-$4f$ line center (T_0) plotted in electron density and temperature space. The values of T_0 are written over the contour lines. Note that for a given N_e and T_0 there may be two possible values of T_e.

plot in Fig. 6 that is consistent with the measured values of N_e and T_0, including the estimated probable errors ($\lesssim 4$ eV) in the ranges of T_e. These probable errors came from uncertainty in the measurements of N_e and T_0 and from uncertainty in the code predictions of T_0.

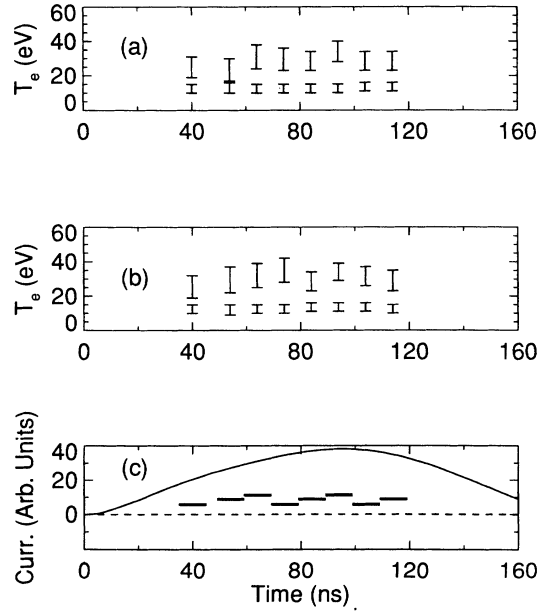

FIG. 7. Results for electron temperature in 8.5-kV (a) and 11-kV (b) discharges in 0.5-mm-diameter capillaries obtained from the measured values of electron density and optical depth at O VI $3d$-$4f$ line center, using the collisional radiative equilibrium code predictions. Current trace (c) with microchannel-plate gate windows (black bars).

Estimates of the ionization time [46] needed to generate an appreciable population of O VI ions argue in favor of T_e being in the upper interval for the first quarter cycle of the discharge. Rapid decay in O VI emission combined with sustained O III emission and a large increase in the background seen in the experimental vacuum-ultraviolet spectra point to a rapid drop of T_e into the lower interval somewhere in the second quarter cycle. Support for this interpretation of the T_e history comes from the results of spatially averaged measurements of the relative intensity histories of O VI $2s$-$2p$, O IV $2s^2 2p$-$2s 2p^2$, and O III $2s^2 2p^2$-$2s 2p^3$ lines. These results showed successive decay of the O VI and O IV lines in the second quarter cycle of the discharge, while the strength of O III emission remained at the same level. They further suggested that since no appreciable O VI emission was seen beyond the first half cycle, the value of T_e for the bulk of the capillary remains in or below the lower interval for the remainder of the discharge.

It is important to note that the ranges of T_e presented here represent a spatial average over the volume of O VI emission in the capillary. For all the observed discharge conditions, these values of T_e were not large enough to be consistent with any appreciable C V or C VI emission from the same volume. This does not eliminate the possibility that some part of the capillary volume is at a much higher T_e (≥ 100 eV), from which C V and/or C VI emission could be observable and O VI emission would be weaker.

B. Anode plasma

Intense time-gated spectra of $\Delta n = 0$ C IV $3s$-$3p$ (580.2- and 581.2-nm) lines were obtained at 45 degrees to the capillary axis of the plasma inside the hollow anode region just outside the capillary [Figs. 1(b) and 8]. These, in conjunction with observations of the nearby C III $3p$-$3d$, 569.6-nm line, provided measurements of the anode-plasma electron density and temperature histories. These plasma conditions were used to estimate the degree of absorption of any C VI H_α line emission in the capillary plasma on passage through the hollow anode. The measurements of the anode plasma concentrated on emission from carbon ions. Intense lines from a number of oxygen impurity ions (O I through O V) fell within the surveyed spectral range, but emission from ionization stages higher than O II was not seen. Electron densities ($N_e \lesssim 2\times 10^{18}$ cm^{-3}) were estimated from Stark widths ($\Delta\lambda_s$) of the C IV $3s$-$3p$, 580.2- and 581.2-nm lines and electron temperatures ($T_e \lesssim 24$ eV) from observed relative line intensity histories of these and the C III ($3p$-$3d$, 569.6 nm) line. These conditions suggested, based on the calculations below, that absorption of any C VI H_α emission in passing through the anode plasma would be negligible ($\sim 10\%$ for a 5-mm-long anode plasma).

1. N_e measurements

The spectra of C III $3p$-$3d$, 569.6-nm and C IV $3s$-$3p$, 580.2- and 581.2-nm lines from the anode plasma were

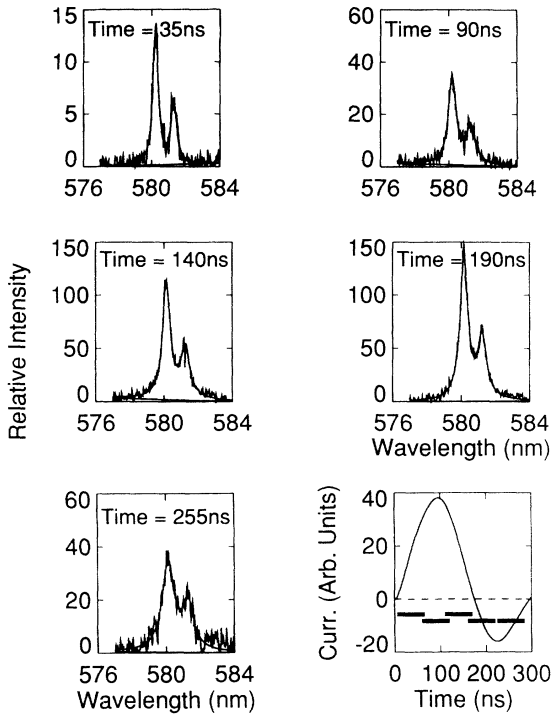

FIG. 8. Voigt profile fits to a sequence of measured time-gated spectra of C IV $3s$-$3p$ 580.2- and 581.2-nm emission from the anode plasma. Current trace with OMA gate windows (black bars).

taken at various times during 8.5-kV discharges in 1-mm-diameter polyacetal capillaries. The fits to Voigt profiles mentioned in Sec. II C, examples of which can be seen in Fig. 8 for C IV, were made using a least squares method [51]. These fits were the convolution of a single instrumental Gaussian and a single Lorentzian profile atop a straight line background. Fit parameters consisted of the measured instrumental FWHM, the Lorentzian FWHM, wavelengths, and strengths of the lines, as well as the slope and intercept of the straight line background. Values for the latter were all extracted from the best fit. All the data points in the fitted wavelength range were given equal weight.

Stark effect was the dominant line broadening mechanism in this plasma, for the C IV $3s$-$3p$ multiplet. Doppler broadening for the estimated ion temperatures ($T_i \approx T_e$, given an electron-ion equilibration time [27] of ~ 1 ns) would contribute less than 1% of the observed linewidths. The C IV $3s$-$3p$ transition was assumed to be optically thin, as evidenced by a near two to one intensity ratio observed (Fig. 8) for the multiplet components. Estimates of Zeeman splitting, the other possible source of broadening [46,50] (assuming $B \leq 5$ kG) also proved negligible. Thus the best fit Lorentzian widths, $\Delta\lambda_L$, of the C IV multiplet components were interpreted as Stark widths, $\Delta\lambda_s$.

Independent measurements of $N_e = (1.5 \pm 0.3) \times 10^{18}$ cm^{-3} and $\Delta\lambda_s = 0.67 \pm 0.04$ nm of the C IV $3s$-$3p$ multiplet components (for $T_e = 7.0 \pm 0.7$ eV) were reported from a gas-liner pinch [52]. These results and the fact that $\Delta\lambda_s$ scales linearly with N_e and only weakly with T_e ($\propto T_e^{-1/2}$) permitted the estimation of a linear scaling relation, $\beta = N_e/\Delta\lambda_s = (2.2 \pm 0.6) \times 10^{18}$ cm^{-3} nm^{-1}, neglecting the effect of the slight difference in T_e from that of the gas-liner pinch.

The results for N_e along with the C IV $3s$-$3p$ fitted relative intensities and the OMA gate times are presented in Fig. 9. They show an increasing trend for N_e over the lifetime of C IV $3s$-$3p$ emission, the latter peaking at ~ 150 ns. The overall uncertainty in N_e was estimated to be $\sim 35\%$. By far the greatest contribution came from the uncertainty in the Stark-broadening scaling parameter β. Minor contributions to the uncertainty included the calibration of the OMA and the suitability of the fits.

2. T_e measurements

The measured relative intensity histories of the C IV (I_1) $3s$-$3p$, 580.2- and 581.2-Å and C III (I_2) $3p$-$3d$, 5696-Å lines were fitted [Fig. 9(b)] by the predictions of a zero-dimensional atomic physics code developed at the University of Maryland [53–55]. A cubic spline fit to the measured N_e history [Fig. 9(a)] was an input to this code. The T_e history was inferred as the fit parameter in the fitting process.

The overall shape of the "best fit" T_e history may be described as that of a step [Fig. 9(a)]. The shape, consisting of an initial somewhat constant high temperature of ~ 19 eV followed by a rapid drop to a much lower, slowly decaying temperature of ~ 6–7 eV, was based on the following: (a) Observations of relatively high electron density and relatively weak C IV $3s$-$3p$ emission of greater intensity than that of C III $3p$-$3d$ at early times (20–100 ns) suggest that the plasma is comprised mainly of ground state C V ions, with few C IV and still fewer C III ions.

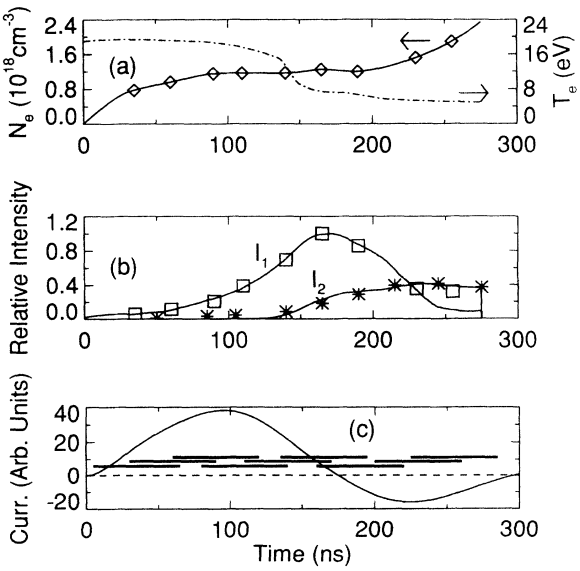

FIG. 9. Code inputs and results for electron density and temperature histories in the anode plasma: (a) Measured electron density history (diamonds), code inputs for electron density (solid line), and temperature (dashed line) histories. (b) Measured C IV $3s$-$3p$ (boxes) and C III $3p$-$3d$, 569.6-nm (asterisks) relative-intensity histories along with the corresponding code predictions (solid lines). (c) Current trace with OMA gate windows (black bars).

This would require a relatively high initial T_e; (b) The fact that C IV $3s$-$3p$ emission grows and peaks before that of C III $3p$-$3d$ is indicative of recombination first from C V into C IV, and later from C IV into C III. Such recombination would require a significant drop from the initial high temperature; and (c) the timing and relative intensities of the peaks dictate the timing and shape of the temperature drop.

Several important aspects of the "best fit" T_e (the early high value of T_e before the drop, the timing and slope of that drop in T_e, and the final low value of T_e) were varied away from that seen in Fig. 9(a) so as to give an indication of the range of T_e history for which the predictions of I_1 and I_2 are compatible with the observations: The range of the early T_e was $\sim 19\pm 3$ eV and that of the late T_e was $\sim 6.0\pm 0.5$ eV. The range of the timing for the drop in T_e was $\sim 150\pm 20$ ns. We also noted that only relatively rapid drops in T_e ($\lesssim 30$ ns wide) gave satisfactory agreement between the measured and the predicted I_1 and I_2.

3. *Implications for* C VI H_α *absorption*

The measured values of T_e and N_e imply a peak absorption of $\sim 5\%$ to 15% of the C VI H_α line, from photoionization of C I through C IV and O II, looking along the capillary axis through a 5-mm-long column of plasma in the anode. These values were estimated using Eq. (5-25) of Ref. [46] for the photoionization cross section per electron. Total photoionization cross sections ($\sigma_{\text{tot}}^{\text{C I}}$ to $\sigma_{\text{tot}}^{\text{C IV}}$ and $\sigma_{\text{tot}}^{\text{O II}}$) for each atom and ion C I through C IV and O II were calculated by summing the individual electron cross sections over all electrons with ionization energies less than $h\nu$ (note that no photoionization of C V or C VI takes place by C VI H_α photons). A total inverse absorption length (η_{tot}) was then estimated from

$$\eta_{\text{tot}} = N_{\text{C I}} \times \sigma_{\text{tot}}^{\text{C I}} + N_{\text{C II}} \times \sigma_{\text{tot}}^{\text{C II}} + N_{\text{C III}} \times \sigma_{\text{tot}}^{\text{C III}} + N_{\text{C IV}} \times \sigma_{\text{tot}}^{\text{C IV}} + N_{\text{O II}} \times \sigma_{\text{tot}}^{\text{O II}} , \quad (6)$$

where the number densities of the carbon atoms and ions ($N_{\text{C I}}$ to $N_{\text{C IV}}$) were predicted by the code for the plasma conditions of N_e and T_e specified above. The number density of oxygen ions ($N_{\text{O II}}$) was not known but was assumed at most to equal the total carbon atom and ion density. The percentage of absorption of C VI H_α emission for a length l of plasma was given by

$$P = 100[1-\exp(-\eta_{\text{tot}} l_{\text{el}})] \approx 5-15\ \% , \quad (7)$$

where $l_{\text{el}} = 5$ mm was assumed equal to the thickness of the graphite electrodes. These values of P would not hinder the passage of H_α emission. Note that for roughly the entire first current half cycle (~ 0–140 ns, $T_e \sim 20$ eV) the higher temperatures imply that a large majority of carbon ions are in the ground state of C V, and do not contribute to photoionization.

IV. SUMMARY AND CONCLUSIONS

A variety of spectroscopic observations of 0.5- and 1-mm-diameter, 1-cm-long, ~ 80-ns current risetime, polyacetal-capillary discharges with energies of between ~ 1 and 20 J have been performed. From these observations we have inferred time-resolved, spatially integrated electron densities and temperatures both inside and outside the capillary. Using these results we estimated that less than 15% of the discharge energy was coupled into forming the plasma. We further estimated [46] that the bulk of the remaining energy coupled into radiation by oxygen ions, which translated into heating the capillary walls and the electrodes.

The bulk of the plasma did not migrate axially beyond the capillary over the lifetime of the discharge. This was evidenced by the fact that oxygen-ion species (O III–O I), whose lines dominated spectra taken axially to the discharge, did not contribute to spectra obtained at 45 degrees in the graphite anode region just outside the capillary (where C III and C IV lines dominated, and where O II lines were detected).

Time-resolved electron temperatures ($\lesssim 25$ eV) and densities ($\lesssim 1.8\times 10^{18}$ cm^{-3}) of the plasma inside the anode were measured from the off-axis spectra. Under those conditions we estimated $\sim 5\%$ to 15% peak absorption (assuming a 5-mm-long column of plasma in the anode) of any C VI H_α emission originating in the capillary.

Measurements of electron temperature and density inside the capillary ($T_e \lesssim 50$ eV and $N_e \lesssim 5.0\times 10^{19}$ cm^{-3} at charging voltages between 3.5 and 11 kV in 0.5- and 1-mm capillaries) based on O VI $3p$-$4d$ and $3d$-$4f$ emission represented a spatial average over the O VI emission volume, and were not consistent [1,38,39] with the pattern of conditions necessary for recombination-pumped gain on the H_α line of C^{5+} (Sec. I). In particular, no evidence was seen for the $\gtrsim 160$-eV electron temperature necessary to fully ionize carbon. The fact that our observations were spatially integrated leaves open the possibility that the necessary conditions are fulfilled in some small portion of the plasma. The measurements of electron density are in good agreement, both in magnitude and general trend, with other results [35].

Towards the end of the first half cycle of the discharge relative intensities of some vacuum ultraviolet lines of O VI, O V, and O IV were observed to undergo successive decays and not to recover intensity in the second or subsequent half cycles. The relative intensity of an O III line was observed to remain relatively constant over the first several cycles of the discharge. These observations were indicative of a drop to even lower temperatures (further from those needed to fully strip carbon) in the bulk of the capillary plasma for the peak of the second half cycle of the discharge—the timing of the reported [32,33] gain bursts.

ACKNOWLEDGMENTS

We would like to thank K. Diller and Professor E. J. Iglesias for their expert technical assistance with this project. We would also like to thank Professor H.-J. Kunze, F. G. Tomasel, Professor J. J. Rocca, and Dr. R. W. Lee for numerous valuable discussions. This work was supported in part by a grant from the National Science Foundation.

[1] R. C. Elton, *X-Ray Lasers* (Academic, San Diego, CA, 1990).
[2] C. J. Keane, in *Ultrashort Wavelength Lasers,* edited by S. Suckewer, SPIE Proc. Vol. 1551 (SPIE, Bellingham, WA, 1992), p. 2.
[3] B. J. MacGowan, L. B. Da Silva, D. J. Fields, C. J. Keane, J. A. Koch, R. A. London, D. L. Matthews, S. Maxon, S. Mrowka, A. L. Osterheld, J. H. Scofield, G. Shimkaveg, J. E. Trebes, and R. S. Walling, Phys. Fluids B **4**, 2326 (1992).
[4] D. J. Nagel, in *Advances in X-ray Spectroscopy,* edited by C. Bonelle and C. Mande (Pergamon, New York, 1982).
[5] S. Suckewer and C. H. Skinner, Science **247**, 1553 (1990).
[6] R. A. McCorkle and H. J. Vollmer, Rev. Sci. Instrum. **48**, 1055 (1977).
[7] A. Zigler, M. Kishenevsky, M. Givon, E. Yarkoni, and B. Arad, Phys. Rev. A **35**, 4446 (1987).
[8] J. J. Rocca, M. C. Marconi, and D. C. Beethe, Opt. Lett. **13**, 565 (1988).
[9] R. C. Elton, J. D. Shipman, and F. C. Young, in *Conference Record-Abstracts, IEEE International Conference on Plasma Science, Oakland, CA, 1990,* IEEE Catalog No. 90CH2857-1 (IEEE, New York, 1990), p. 108.
[10] U. Fisher, H. Jäger, and W. Lochte-Holtgreven, Phys. Lett. **44B**, 161 (1973).
[11] W. Lochte-Holtgreven (unpublished).
[12] W. Lochte-Holtgreven, Atomkernenergie **28**, 150 (1976).
[13] S. K. Händel and O. Jonsson, Atomkernenergie/ Kerntechnik **36**, 170 (1980).
[14] R. A. McCorkle, Nucl. Instrum. Methods **215**, 483 (1983).
[15] R. A. McCorkle, Nuovo Cimento B **77**, 31 (1983).
[16] J. D. Sethian, K. A. Gerber, and A. E. Robson, Bull. Am. Phys. Soc. **30**, 1388 (1985).
[17] P. Bogen, H. Conrads, and D. Rusbüldt, Z. Phys. **186**, 240 (1965).
[18] P. Bogen, H. Conrads, G. Gatti, and W. Kohlhaas, J. Opt. Soc. Am. **58**, 203 (1968).
[19] S. M. Zakharov, A. A. Kolomenskii, S. A. Pikuz, and A. I. Samokhin, Pis'ma Zh. Tekh. Fiz. **6**, 1135 (1980) [Sov. Tech. Phys. Lett. **6**, 486 (1980)].
[20] R. A. McCorkle, Appl. Phys. A **26**, 261 (1981).
[21] V. I. Bayunov, E. M. Golubev, N. N. Ogurtsova, and I. V. Podmoshenskii, Opt. Spektrosk. **53**, 1114 (1982) [Opt. Spectrosc. (USSR) **53**, 666 (1982)].
[22] S. N. Belov, E. M. Golubev, N. N. Ogurtsova, I. V. Podmoshenskii, E. V. Priemysheva, and E. G. Vinokurova, in *X-Ray Instrumentation in Medicine and Biology, Plasma Physics, Astrophysics, and Synchrotron Radiation,* edited by R. Benattar, SPIE Proc. Vol. 1140 (SPIE, Bellingham, WA, 1989), p. 28.
[23] E. G. Vinokurova, E. M. Golubev, and V. P. Ugarova, Opt. Spektrosk. **66**, 1244 (1989) [Opt. Spectrosc. (USSR) **66**, 724 (1989)].
[24] A. W. DeSilva and H. J. Kunze (unpublished).
[25] A. W. DeSilva (private communication concerning experiment in progress at the University of Maryland involving exploding wires in capillaries).
[26] A. M. Howaston, *An Introduction to Gas Discharges* (Pergamon, New York, 1965).
[27] D. L. Book, NRL Report No. 177-4405, 1990 (unpublished).
[28] G. A. Guzdenko and L. A. Shelepin, Zh. Eksp. Teor. Fiz. **45**, 1445 (1963) [Sov. Phys. JETP **18**, 998 (1964)].
[29] D. Jacoby, G. J. Pert, S. A. Ramsden, L. D. Shorrok, and G. J. Tallents, Opt. Commun. **37**, 193 (1981).
[30] S. Suckewer, C. H. Skinner, H. Milchberg, C. Keane, and D. Voorhees, Phys. Rev. Lett. **55**, 1753 (1985).
[31] C. H. Skinner, D. Kim, E. Valeo, and A. Wouters, Phys. Rev. Lett. **57**, 1004 (1986).
[32] C. Steden and H.-J. Kunze, Phys. Lett. A **151**, 534 (1990).
[33] C. Steden, H. T. Wieschebrink, and H.-J. Kunze, in *Proceedings of the 3rd International Colloquium on X-ray Lasers, Schliergee, Germany, 1992,* edited by E. E. Fill, IOP Conf. Proc. No. 125 (Institute of Physics, Philadelphia, 1992), p. 423.
[34] C. A. Morgan, University of Maryland Report No. UMLPR 93-022, 1993 (unpublished).
[35] F. G. Tomasel, J. J. Rocca, O. D. Cortázar, B. Szapiro, and R. W. Lee, Phys. Rev. E **47**, 3590 (1993).
[36] J. Ashkenazy, R. Kipper, and M. Carner, Phys. Rev. A **43**, 5568 (1991).
[37] N. Edison, P. E. Young, N. Holmes, R. W. Lee, N. C. Woolsey, J. S. Wark, and W. J. Blyth, Phys. Rev. E **47**, 1305 (1993).
[38] R. C. Elton, Opt. Eng. **21**, 307 (1982).
[39] R. C. Elton, Comments At. Mol. Phys. **13**, 59 (1983).
[40] H. Shin, D. Kim, and T. N. Lee, Bull. Am. Phys. Soc. **37**, 1502 (1992).
[41] J. J. Rocca, M. C. Marconi, B. T. Szapiro, O. Buccafusca, and K. Richardson (private communication).
[42] J. J. Rocca, O. D. Cortázar, B. Szapiro, K. Floyd, and F. G. Tomasel, Phys. Rev. E **47**, 1299 (1993).
[43] J. S. Wang, H. R. Griem, Y. W. Huang, and F. Böttcher, Phys. Rev. A **45**, 4010 (1992).
[44] J. S. Wang, H. R. Griem, and E. J. Iglesias, Phys. Rev. A **40**, 4115 (1989).
[45] R. L. Kelly, J. Phys. Chem. Ref. Data **16**, Suppl. 1 (1987).
[46] H. R. Griem, *Plasma Spectroscopy* (McGraw-Hill, New York, 1964).
[47] H.-J. Kunze, Phys. Rev. A **4**, 111 (1971).
[48] H.-J. Kunze and W. D. Johnston III, Phys. Rev. A **4**, 962 (1971).
[49] O. Bely and D. Petrini, Astron. Astrophys. **6**, 318 (1970).
[50] H. R. Griem, *Spectral Line Broadening by Plasmas* (Academic, New York, 1974).
[51] P. R. Bevington, *Data Reduction and Error Analysis for the Physical Sciences,* 1st ed. (McGraw-Hill, New York, 1969).
[52] S. Glenzer, N. I. Uzelac, and H.-J. Kunze, Phys. Rev. A **45**, 8795 (1992).
[53] H.-J. Kunze, A. H. Gabriel, and H. R. Griem, Phys. Rev. **165**, 267 (1968).
[54] B. L. Welch, Ph.D. thesis, University of Maryland, 1991.
[55] S. W. Daniels, Ph.D. thesis, University of Maryland (1991).

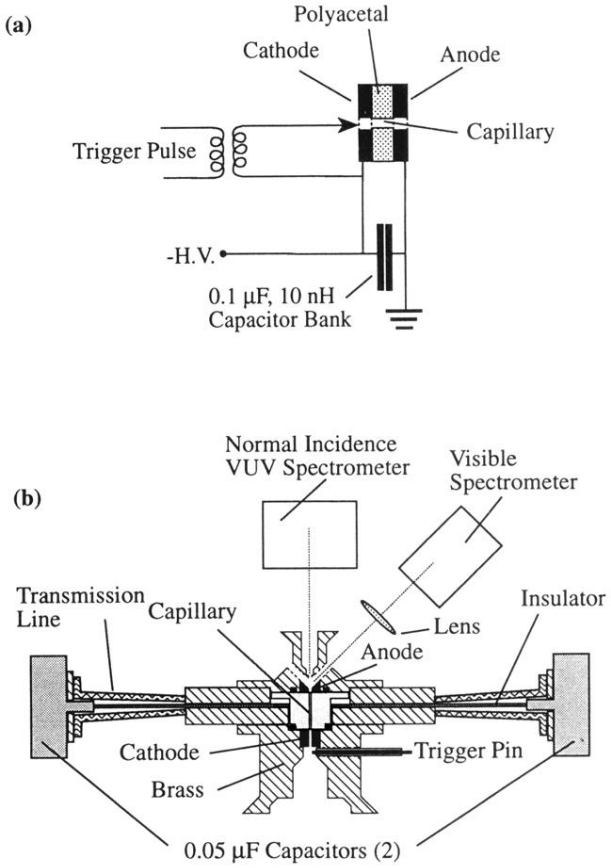

FIG. 1. Circuit (a) and experimental setup (b).